RESULTS FROM THE K2K EXPERIMENT

Yoshinari Hayato
Institute of Particle and Nuclear Studies,
High Energy Accelerator Research Organization,
1-1 Oho, Tsukuba, Ibaraki, Japan
Representing the K2K Collaboration

ABSTRACT

The KEK to Kamioka (K2K) long baseline neutrino oscillation experiment has been successfully started since March 1999. This is the first accelerator-based long baseline neutrino oscillation experiment, and this experiment is expected to cover most of the parameter regions of neutrino oscillation which have been suggested by various atmospheric neutrino experiments. The neutrino beam is very stable, as confirmed by the secondary beam monitors and neutrino detectors located at KEK. The spectrum and profile of the neutrino beam is estimated by the newly developed pion monitor, which is one of the secondary particle monitors, and the obtained results are in good agreement with the results obtained from our Monte Carlo simulations. The accumulated number of protons on target is 2.29×10^{19} and the estimated expected number of fully contained events at Super-Kamiokande is $40.3^{+4.7}_{-4.6}$ in the case of no oscillation. The observed number of events at Super-Kamiokande is 27, which is $2\,\sigma$ off from the expected number of events.

1 Introduction

The standard model of electroweak interactions[1] is one of the most successful models in particle physics. In this model, the mass of the neutrino is defined to be zero. Therefore, it has a large impact on the standard model and requires extensions of it, if masses of neutrinos are proven to be nonzero. Since the late 1980s, some experiments on atmospheric neutrinos have reported deficits of ν_μ with energies around 1 GeV.[2–4] In 1998, the Super-Kamiokande collaboration not only confirmed a deficit of atmospheric ν_μ with high statistics, but they also reported a clear zenith angle dependence of the deficit.[5] This means that the disappearance probability of ν_μ depends on the distance between point where the neutrino was created and the detector. These experimental results are well explained by neutrino oscillation and imply that neutrinos should have non-zero masses. Therefore, it became very important to investigate the various characteristics of neutrino oscillation. For that purpose, several long baseline neutrino experiments, which use accelerators as the neutrino source, have been proposed. Among of them, the KEK to Kamioka (K2K) long baseline neutrino oscillation experiment is the first accelerator-based experiment to study the atmospheric neutrino oscillation.[6] The main purpose of this experiment is to confirm the ν_μ disappearance and to search for the ν_e appearance by neutrino oscillations. This experiment is able to cover almost all the parameter regions which are suggested by the results from atmospheric neutrino analysis. (See Fig. 1.) Because this kind of experiment will provide us with a way to study flavor mixing in the lepton sector, it is also important for the K2K experiment to establish various experimental methods of accelerator-based long baseline neutrino oscillation experiments, such as alignment, aiming of the neutrino beam, monitoring the stability of the beam, and so on.

In the first stage of the K2K experiment, the indication of neutrino oscillations is expected to be identified as a deficit of the observed number of neutrino interactions at Super-Kamiokande. Therefore, it is very important to estimate the expected number of events at Super-Kamiokande precisely. In order to estimate accurately the expected number of interactions at Super-Kamiokande, we have to understand the characteristics of the neutrino beam well. For that purpose, we have developed various kinds of primary and secondary beam monitors and neutrino detectors. In the following sections, we'll describe the beam monitors and detectors briefly and summarize the results from each detector including Super-Kamiokande.

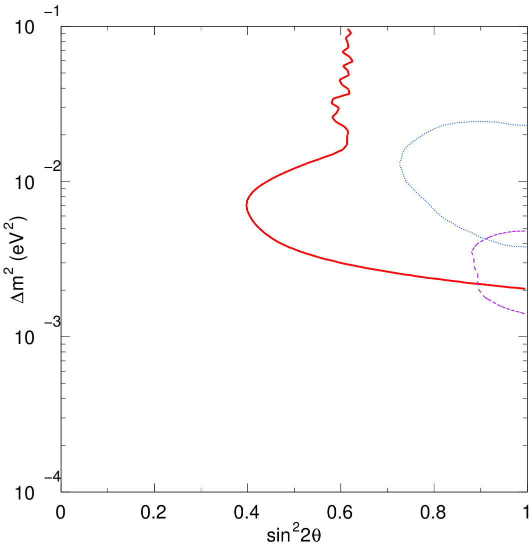

Fig. 1. Allowed parameter regions of neutrino oscillation ($\nu_\mu \rightarrow \nu_\tau$ or $\nu_{\rm s}$) and the sensitive region of the K2K experiment. The dashed (dotted) line shows the 90% C.L. allowed region obtained by the Super-Kamiokande (Kamiokande) experiment. The solid line shows the 90% C.L. sensitive region of the K2K experiment (for 10^{20} protons on target).

2 Overview of the K2K experiment

The K2K experiment is the first accelerator-based long baseline neutrino oscillation experiment. The schematic view of this experiment is shown in Fig. 2.

The neutrinos are generated and monitored at KEK in Tsukuba, travel through the Earth for 250 km, and are detected by the Super-Kamiokande detector located underground in the Kamioka mine, Gifu. The K2K neutrino beam is a horn-focused wide band beam, and is nearly pure ν_μ beam (98.2% ν_μ, 1.3% ν_e and 0.5% $\bar{\nu_\mu}$). The mean energy of the neutrino is about 1.3 GeV.[7] The oscillation probability for the two-flavor approximation can be written as follows:

$$P(\nu_\mu \rightarrow \nu_x) = \sin^2 2\theta \cdot \sin^2(1.27 \Delta m^2 L/E_\nu), \tag{1}$$

where P is the oscillation probability, θ is the mixing angle, Δm^2 is the squared mass difference, L is the travel length of the neutrino (baseline distance), and E_ν is the energy of the neutrino. As described above, the baseline(L) is 250km and the mean energy of neutrinos(E_ν) is about 1.3GeV for the K2K experiment. Therefore, we can investigate the parameter regions where $\Delta m^2 \geq 2 \times 10^{-3}$ eV.

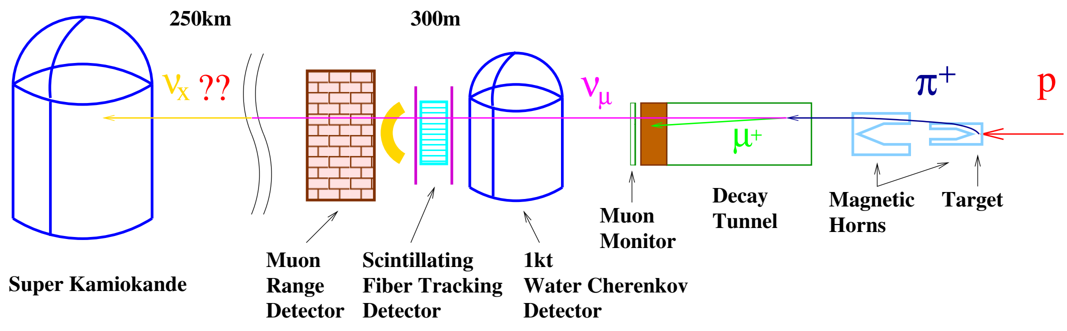

Fig. 2. Schematic view of K2K experiment. See text for detail.

The neutrino beam is generated from the decay of pions. In order to generate charged pions, we use proton Al interactions. The primary protons are extracted from the 12 GeV proton synchrotron at KEK every 2.2 sec.[8] The total width of a spill is about 1.1 μs and there are 9 bunches in a spill. The total number of protons is about 5.5×10^{12} per spill. The protons are extracted to the north direction and are bent by 90 degrees west, in which direction Super-Kamiokande detector is located. The target to generate pions is made of aluminum and its size is 30mm (25mm in June, 1999) in diameter and 660mm in length. This target is embedded in the first magnetic horn which focuses the generated positive pions and sweeps out the negative charged particles.[9] After the first horn, there is the second magnetic horn in order to make the parallel pion beam. These two horns are driven with pulsed 250 kA current (200 kA in June 1999) whose width is 2 ms. After the horns, there is a decay tunnel whose length is 200 m and which is filled with 1 atm He gas. The pions generated at the target decay into muons and neutrinos, and the muons decay into positrons and neutrinos while traveling in this tunnel. After the decay tunnel, there is a beam dump, which absorbs all the hadronic components and low energy muons. We put two muon monitors in the muon pit just after this beam dump to measure the direction of the beam by the muons which passed through the dump. Between the muon pit and the front neutrino detectors, there is 10 m of soil and all the remaining muons are absorbed. Therefore, only neutrinos reach the front neutrino detectors. We placed three different types of neutrino detectors. One is the 1 kt water Cherenkov detector. This is a miniature of Super-Kamiokande. The second one is the scintillating fiber tracking detector. This detector consists of 20 layers of scintillating fibers for particle detection, and water containers as the target material. The coverage of this detector is relatively small, 2.2 m$\times$2.2 m. However, the resolution of the vertices and particle trajectory reconstructions are much better, compared to the other front detectors. Moreover, this detector is able to detect the tracks of low momentum charged particles, such as protons or pions, which cannot be observed by the water Cherenkov type detectors, and thus we can investigate the neutrino interactions in detail. The last detector is the muon range detector. This detector consists of 12 layers of iron absorbers and 6632 muon drift tubes. This detector covers a very large area (7.6 m×7.6 m) and we can monitor the profile of the neutrinos and energy spectrum with a few days of data. By using this detector, we can confirm the stability of the neutrino beam by neutrino interactions.

As the far neutrino detector, we use the Super-Kamiokande detector. This is the world largest ring imaging water Cherenkov detector, whose fiducial volume is 22.5 kt. This detector is located at the Mozumi zinc mine near Kamioka, Japan, at a distance of 250 km from KEK. Super-Kamiokande has been running since April 1996 and neutrino interactions have been extensively studied with this detector. Therefore, it is very suitable for a long baseline experiment.

The overall alignment of the equipment is essential in a long baseline neutrino experiment.[10] In the case of the K2K experiment, the divergence of the neutrino beam at Super-Kamiokande has been estimated by Monte Carlo simulation and it was almost flat within 3 mrad. (See Fig. 3.)

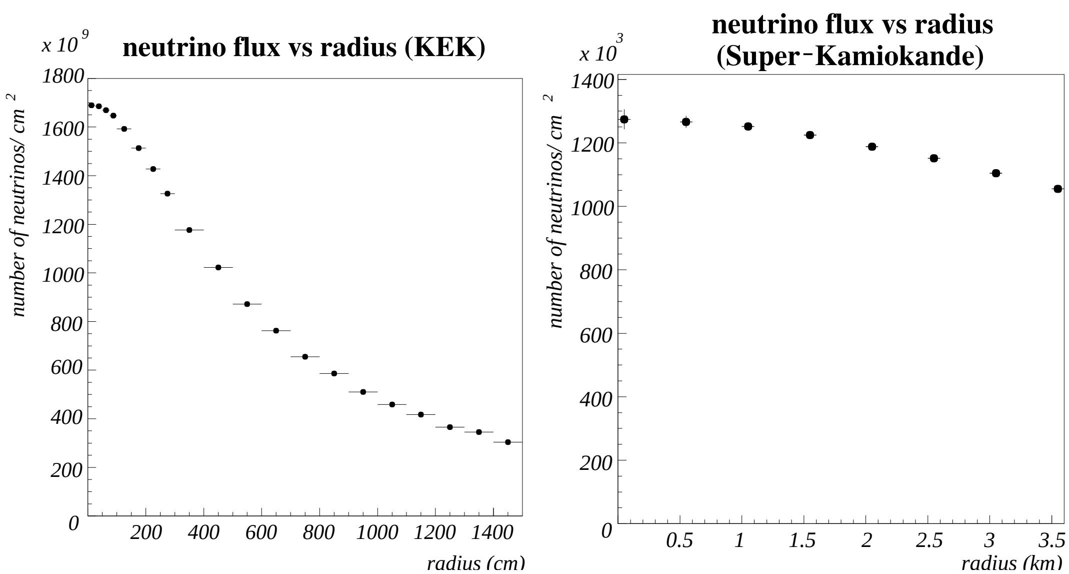

(A) (B)

Fig. 3. Neutrino profiles at (A) near detector (KEK) and (B) far detector (Kamioka). These plots are made using the K2K standard beam Monte Carlo simulation.

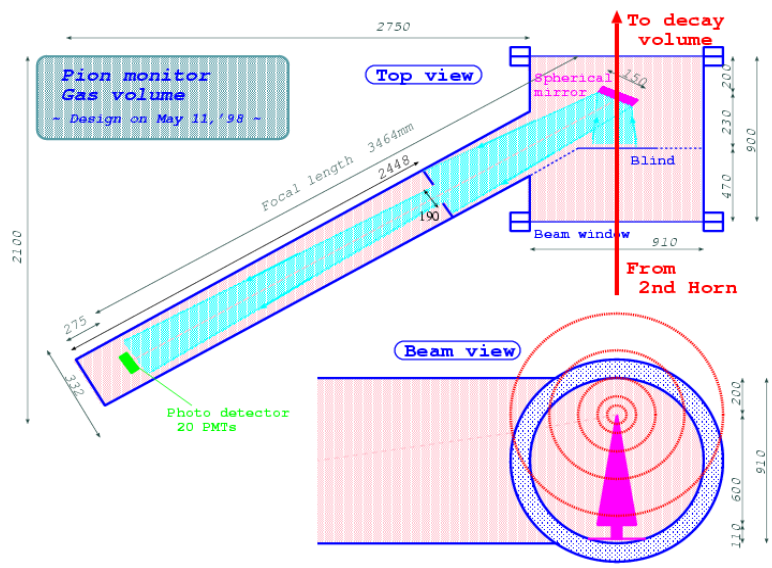

Fig. 4. Schematic view of the pion monitor. See text for detail.

Therefore, it is necessary for us to align everything much better than this tolerance. The actual alignment has been done with a GPS survey and all the equipment including target, magnetic horns, decay tunnel and all the detectors, were adjusted with an accuracy of 0.1 mrad, which is good enough for this experiment.

We started taking data in March 1999 and checked the components. The physics run started in June 1999. Since then, 2.3×10^{19} protons have been delivered on target.

3 Results from the secondary beam monitors

The secondary beam monitors[11] provide us with various important information about the neutrino beam. We use the data from the pion monitor to estimate the flux of neutrinos in KEK and at Super-Kamiokande. Muon monitors make it possible to adjust and monitor the direction of the beam spill by spill.

3.1 Pion monitor

The pion monitor is a threshold type gas Cherenkov detector and was developed to measure the energy spectrum and directional distributions of charged pions. A schematic view of the pion monitor is shown in Fig. 4. Usually, the pion monitor is located a little bit away from the beamline; we place this detector in the middle of the beamline only when we try to take data.

Cherenkov photons are emitted from charged particles whose velocity is faster than the speed of the light in the medium. The relation between the direction of the emitted Cherenkov photon and the direction and momentum of the charged particle can be written as:

$$\cos(\theta) = \frac{1}{n\beta}, \qquad (2)$$
$$\beta \equiv \frac{p}{E},$$

where θ is the angle between the direction of the Cherenkov photons and the direction of the charged particle, n is the refractive index of the medium, and p and E are the momentum and energy of the charged particle, respectively. If it is possible to change the refractive index of the medium in the detector, we can change the threshold momentum of the particle to be detected. We selected a Freon gas as the medium of the detector because the refractive index of the Freon gas is appropriate for our measurement and is easily controlled by changing the pressure of the gas.

Cherenkov photons emitted from the pions are reflected by the spherical mirror located at the end of the gas volume, and are detected by the Photo Multiplier Tube(PMT) array. This PMT array consists of 20 1/2 inch PMTs located on the focal plane of the spherical mirror. Because of the characteristic of a spherical mirror, the image at the focal plane reflects the incoming direction of the photons and does not depend on the position of the photons at the mirror. This means that the location of the image of the Cherenkov light observed at the focal plane corresponds to the direction of the charged particle, and the distance between the two peaks of the image corresponds to the opening angle of the Cherenkov light. The observed charge distributions of the pion monitor with various refractive indices are shown in Fig. 5. We can see clearly two peaks of Cherenkov light, and the distance between the two peaks changes according to the refractive indices. Unfortunately, we can not lower the Cherenkov threshold below $P_\pi \leq 2\,\text{GeV}$ because primary $12\,\text{GeV}$ protons begin to emit Cherenkov photons in such a high refractive index region.

From these distributions, we can reconstruct the momentum and directional distributions of charged pions by fitting. Once we know the momentum and directional distributions of the pions, we can easily estimate the neutrino fluxes by assuming the decay kinematics of the pions. The obtained fluxes are shown in Fig. 6. Here the absolute normalizations of the fluxes are arbitrary. According to these results, our stan-

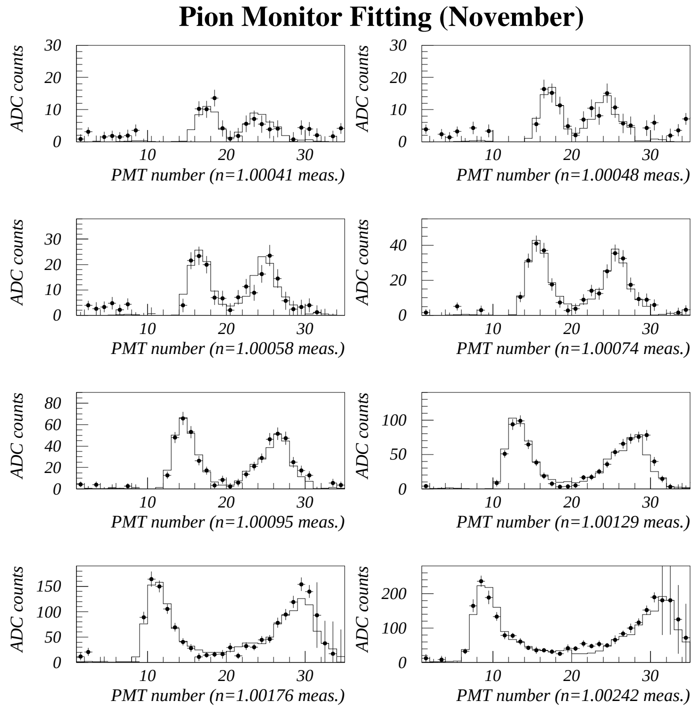

Fig. 5. Observed charge distributions from the pion monitor for different refractive indices. The circles with error bars show the data and the error bars correspond to the statistical error. The histograms show the fitted results. See text for detail.

dard beam Monte Carlo program reproduces the flux obtained from the pion monitor well. Our standard beam Monte Carlo is based on GEANT.[12] In order to simulate the primary proton interactions on aluminum, we use the parameters based on various experimental results of hadron production.[13] The other hadronic interactions are treated by GCALOR.[14]

3.2 Muon monitors

There is a muon dump after the decay tunnel. We placed two types of muon profile monitors after the muon dump: a silicon pad detector and a large area ionization chamber. (See Fig. 7.) The muon dump consists of 3.5 m of iron and 2 m of concrete. While passing through this dump, all the hadronic components are absorbed and only the high energy muons, whose momentum is more than 5.5 GeV/c at the end of decay tunnel, reach the muon monitors. The profile of these energetic muons is known to be well correlated with the profile of the neutrino beam, and there are enough muons in a spill

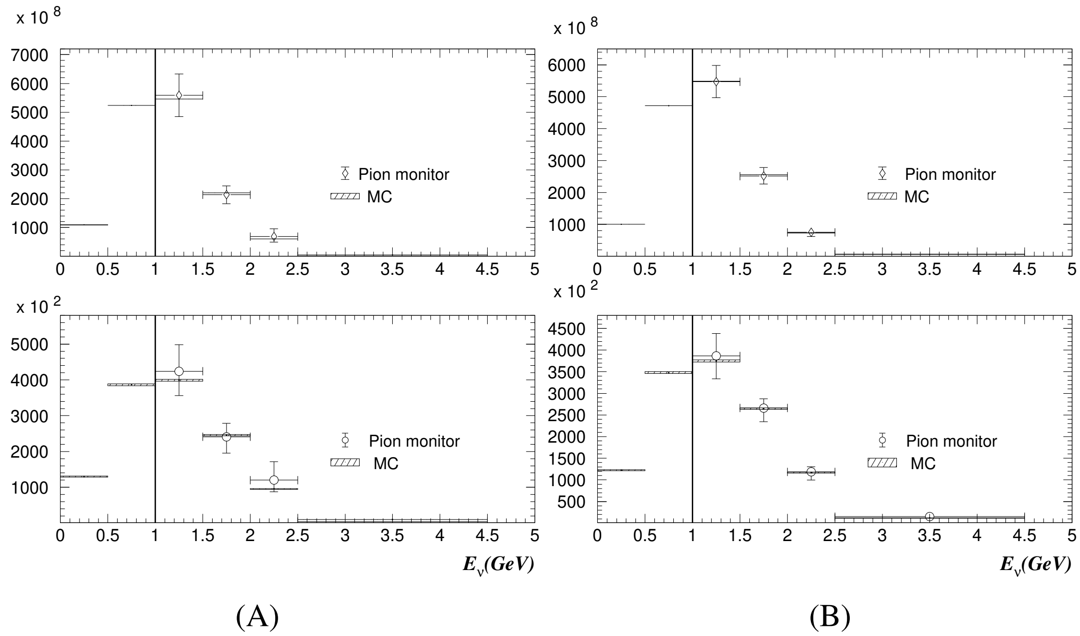

Fig. 6. Estimated neutrino spectrum for the configuration used in June '99 (A) and configuration used after Nov. '99 (B). Upper figures show the estimated flux at KEK and the lower figures show the estimated flux at Super-Kamiokande. The open circle with error bars corresponds to the results from the pion monitor; error bars include systematic errors. The hatched boxes show the Monte Carlo expectation, and the size of each box corresponds to the error.

for the profile measurement. Therefore we can adjust the direction of the beam using the observed profile of muons, and also monitor the direction of the beam spill by spill.

The ionization chamber (μ-SPIC) consists of six planes of Ar chambers, whose coverage is 2 m$\times$2 m, and the size of each chamber is 60 cm$\times$90 cm. Inside the chamber, there are two readout planes, one in the horizontal and the other in the vertical plane. Between these two readout planes, there is a high voltage plane in the middle of the two readout planes, and the distance between the central plane and one of the readout planes is 1 cm. There are 32 strips in the horizontal plane and 36 strips in the vertical plane. The width of each strip is 5cm. Each of the strip is connected to the corresponding strip in the neighboring chambers. Thus, these six chambers act as one large chamber. Fig. 8 shows the time variation of the fitted center of muons observed by this detector. It shows that the beam center is stable within 1mrad in the X and Y directions. In order to confirm the results from the ionization chamber, we prepared the other muon mon-

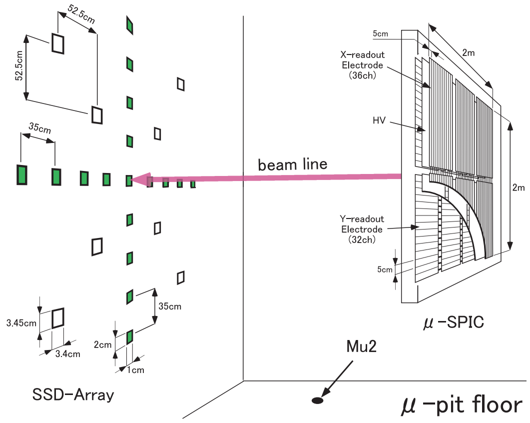

Fig. 7. Schematic view of the muon monitors. See the text for details.

itor, which has a coarse grain but is expected to be stable. We placed 26 silicon pad detectors on the wall behind the ionization chamber (SSD-Array). Seventeen of them are 10 mm×20 mm and 9 of them are 34 mm×34.5 mm. The obtained distributions are consistent with the results from ionization chamber.

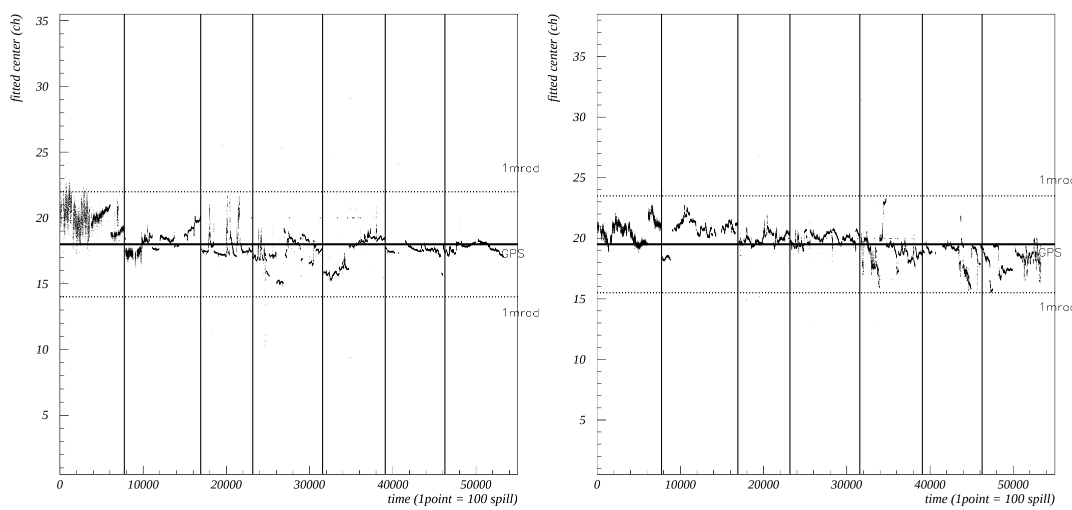

(A) (B)

Fig. 8. Fitted center of the muons monitored by the ionization chamber in the muon pit. The variation of the center of the beam is confirmed to be less than 1 mrad.

4 Results from the neutrino detectors

In order to measure the generated neutrino fluxes and spectrums at KEK, we use three different types of neutrino detectors: water Cherenkov detector, scintillating fiber tracking detector[15] and muon range detector.[16] Each of them has different characteristics and thus we can check the consistency of our measurements, and it allows us to investigate the neutrino interactions more precisely. (See Fig. 9.)

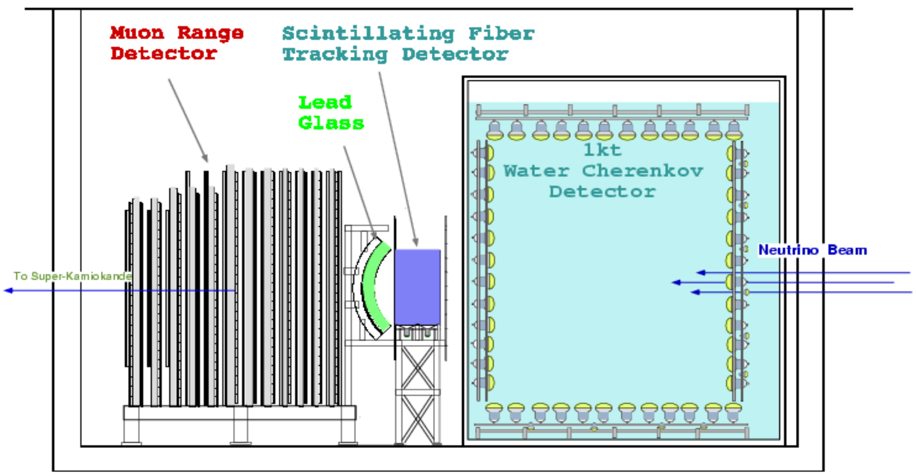

Fig. 9. Front neutrino detectors. See text for detail.

There is also a lead-glass detector to search for ν_e but this detector is not used for the ν_μ flux measurement. For the estimation of the expected number of events at Super-Kamiokande, we decided to use the results from the water Cherenkov detector as the reference value. Because these two detectors are of the same type, several systematic errors are cancelled. However, we don't have enough statistics from the water Cherenkov detector to monitor the stability of the neutrino beam in a period of only a few days. The muon range detector is suitable for this kind of monitoring. The coverage of the muon range detector is about 7 m$\times$7 m and the fiducial mass of this detector is several times larger than that of the 1 kt water Cherenkov detector. Therefore, we can check not only the stability or time dependence of the event rate, which is directly related to the absolute flux, but also the stability of the energy spectrum of the neutrinos.

In order to estimate the detection efficiency for neutrino-induced events, contamination of the backgrounds and various systematic errors, we used Monte Carlo simulated events. The neutrino interaction part of the simulation is basically the same which is used in Super-Kamiokande.

4.1 Muon range detector

The muon range detector consists of the drift chambers and 12 iron plates. The size of the detector is about 7.6 m in width and 7.6 m in height. There are two layers of drift chambers in both the X and Y directions, for a total of 4 layers, equipped on both sides of each iron plate. In order to get better energy resolution, the upstream 4 iron plates are 10 cm thick and the downstream 8 plates are 20 cm thick. The total thickness of iron is 2.0 m and it is possible to measure up to 2.8 GeV/c muons. We use 829 drift chamber modules, each of which has 8 independent cells. The size of each cell is 50 mm$\times$70 mm. In total, there are 6632 drift tubes and all the channels are read out by TDC modules. By using the timing information, we can reconstruct the particle trajectory precisely; the typical resolution obtained is less than 1 cm. As for the momentum reconstruction, there is no way to identify the interaction point of the neutrino in the iron plate or the stopping position of the particle. Therefore, the resolution of the reconstructed momentum of a muon is about 120 MeV.

In order to select the neutrino-induced events, we apply the following cuts after track-finding:
a) each track does not share a vertex with other tracks,
b) the tracks have to be generated within the beam spill timing,
c) both ends of the tracks have to be contained within the detector,
d) either endpoint of each track should be in one of the upstream 9 iron plates.
Criterion a) is used to avoid double-counting the number of interactions. Criterion b) is used to eliminate the cosmic-ray background events. Criterion c) is used to select the events which were generated within the detector. For the profile measurement of the neutrino interactions, we apply an additional cut, which rejects the events whose reconstructed energy is less than 0.5 GeV or greater than 2.5 GeV. These events are rejected because the acceptance of these high energy and low energy events depends on the interaction vertex, and the differences are quite large even in the fiducial volume. Typical profiles of the neutrino beam are shown in Fig. 10. The Monte Carlo prediction reproduces these profiles very well. By fitting the profile, we can monitor the time dependence of the ν_μ beam. As shown in Fig. 11-(A), the ν_μ beam is well centered and very stable within 1 mrad. We can also measure the neutrino event rate and the

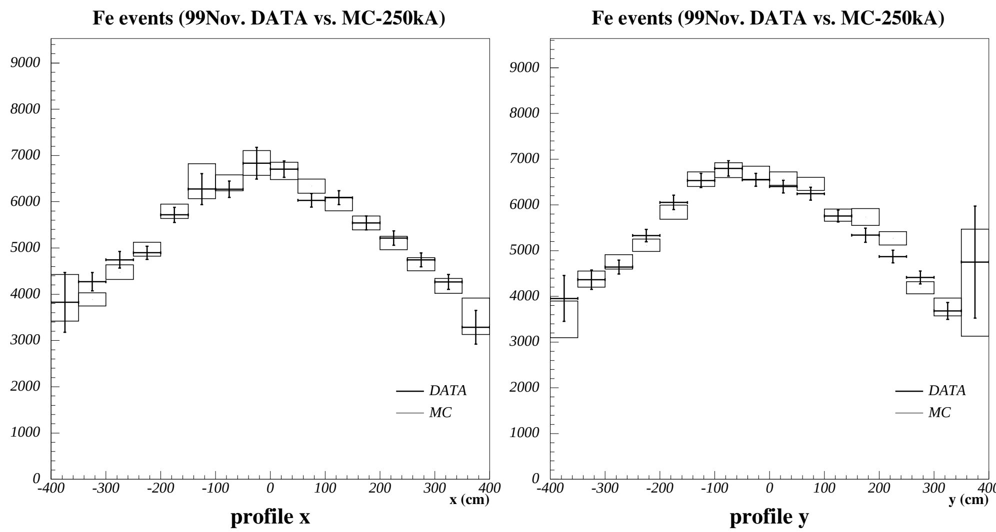

(A) (B)

Fig. 10. Typical vertex distributions of neutrino interactions (profile of neutrino beam) at the muon range detector. Fig. A (B) shows the horizontal (vertical) distribution. Each cross shows the data and error. The boxes correspond to the Monte Carlo predictions.

spectrum. For this analysis, we defined a cylindrical fiducial volume, whose radius is 3 m and the total fiducial mass is 312 tons. The typical event rate is about 0.05 events/spill, and thus we have enough events to monitor the stability on a daily basis. The time dependence of the neutrino event rate in this detector is shown in Fig. 11-(B) and it is very stable. In June '99, we used a different configuration of the target and horns, for which the event rate is slightly lower than the other periods.

It is also possible for us to measure the angular and direction distributions of the muons. These distributions are very sensitive to the neutrino spectrum. The results are shown in Fig. 12. These figures show no time dependence, and so the stability of the neutrino beam spectrum was also confirmed.

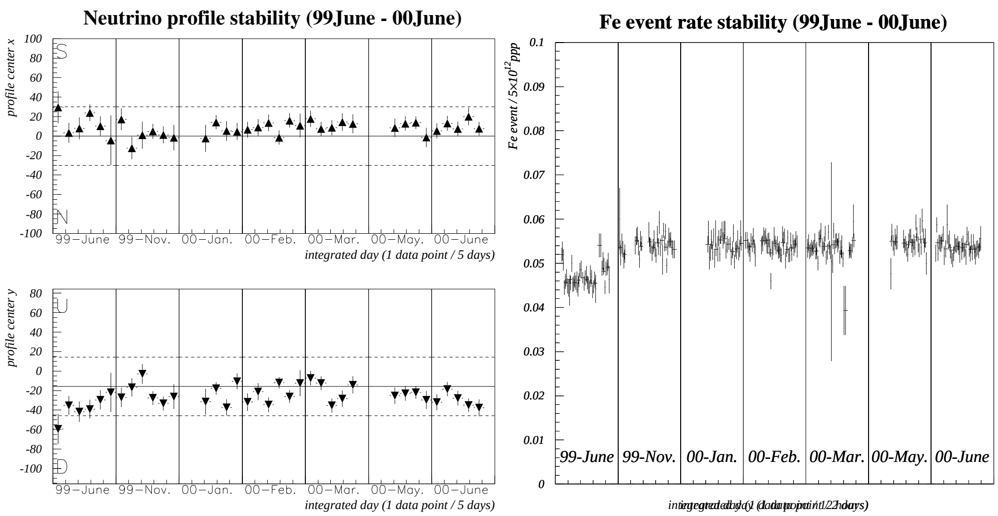

(A) (B)

Fig. 11. Time dependences of (A) the center of neutrino beam and (B) the neutrino event rate monitored by the muon range detector for all the experimental period. The upper (lower) figure of (A) shows the horizontal (vertical) distribution. The dashed lines in each figure of (A) show the position away from 1 mrad. Each error bar shows the statistical error.

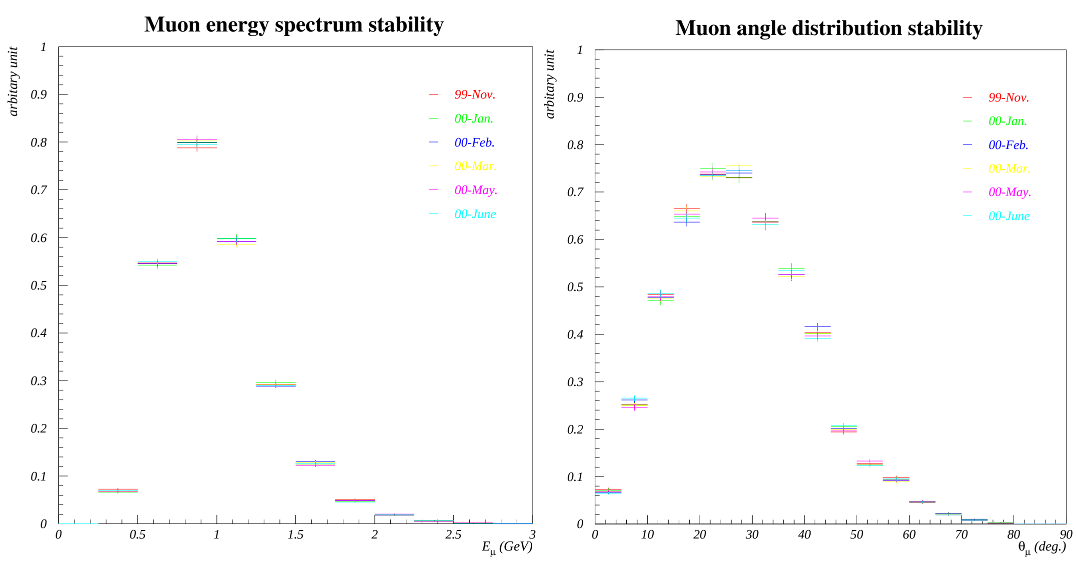

Fig. 12. Momentum and angular distributions of muons observed by the muon range detector. Each cross corresponds to one month of data.

4.2 Scintillating fiber tracking detector

The scintillating fiber tracking detector consists of 20 layers of 2.6 m$\times$2.6 m tracking modules and 19 layers of water containers. Each tracking module consists of two scintillating fiber sheets for horizontal and vertical directions. Each scintillating fiber sheet has two layers to improve the particle detection efficiency. The diameter of the scintillating fiber is 0.7 mm and the length is 3.7 m. The water containers were made of 1.8 mm thick aluminum, and have a size of 16 cm$\times$240 cm$\times$6 cm. Fifteen tanks are used for one target layer. The scintillating fibers are combined and read out by 24 Image Intensifier Tubes (IITs). The IIT is an imaging detector which uses a CCD for the final readout. We have also prepared a special 8 bit depth Flash ADC (FADC) module and FIFO module to readout entire CCD images from each IIT. We can identify the individual fibers through which particles passed, and we reconstruct the tracks with this information. However, the gate width of each IIT needs to be set to more than 0.1 μsec to match the decay time of the phosphor screen. Therefore, we need trigger counters to eliminate cosmic-ray muons. For that purpose, we have also prepared two large trigger counters located both upstream and downstream of this detector. Each of the trigger counters consists of 40 scintillators and its size is 407 cm$\times$400 cm, which is large enough to cover the entire scintillating fiber tracking detector. The size of each scintillator is 407 cm$\times$10.5 cm$\times$4.2 cm. For the upstream detector, we connect two scintillators with one lightguide and treat them as one large module. For the downstream counter, we need higher resolutions for both position and energy, so each scintillator is read out independently. Each of the scintillator modules is equipped with two PMTs on both sides and we can easily reconstruct the location with the obtained charge and timing information.

This time we select neutrino events which have vertices in the detector volume, and the exiting muon must generate a track in the muon range detector. With this data sample, we can check the consistency of the event rate and distributions of energy and direction of the muons by comparing the results from the two detectors, the scintillating fiber tracking detector and the muon range detector, which use different target material. The actual event selection criteria are defined as follows:

a) there is no hit in the upstream counter,

b) the track penetrates more than two layers of the tracking modules,

c) the vertex (starting point) of the track must be in the fiducial volume,

d) there must be corresponding hits in the downstream trigger counter,

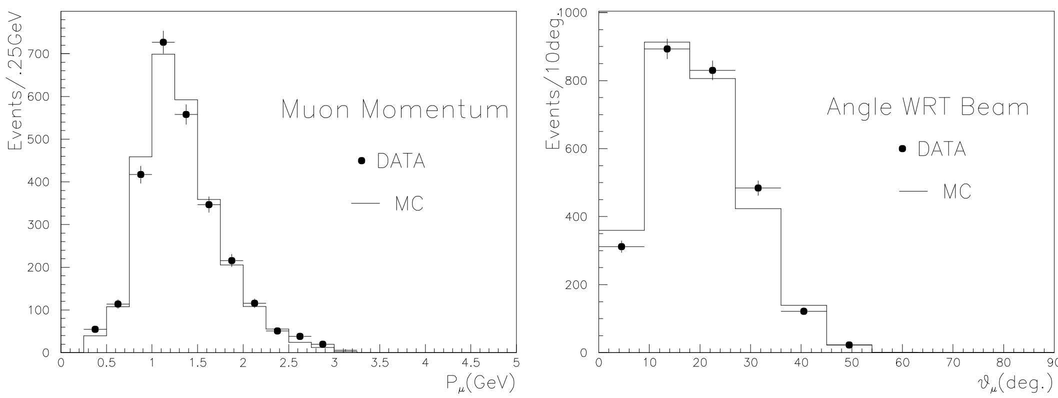

(A) (B)

Fig. 13. (A) Momentum and (B) angular distributions of muons from the scintillating fiber tracking detector. The filled circles with bars show the data. Each error bar shows statistical errors. The histograms show the Monte Carlo simulation.

e) the track found in the detector must be connected to the track in the muon range detector.

Criterion a) is used to reject the incoming cosmic ray muons. Criterion b) is used to reject noise tracks. Criterion c) is used to select the vertex-contained samples. Criteria d) and e) are used to select the tracks which have corresponding tracks in the muon range detector. After applying all these cuts, 2953 events remain. The event rate is about 8.3×10^{-4} events/spill and the expected interaction rate estimated by using the Monte Carlo is consistent with the other two detectors. The angular and momentum distributions of the muons are shown in Fig. 13. The results from the Monte Carlo reproduce the data well.

4.3 1 kt Water Cherenkov detector

The 1 kt water Cherenkov detector is a miniature of the Super-Kamiokande detector. This detector consists of a cylindrical water tank, which can hold 1 kt of pure water and 680 20 inch PMTs. Each charged particle generates one Cherenkov ring in this detector, and thus we can count the number of charged particles by counting the number of Cherenkov rings. As for the reconstruction of the direction of each particle, we can use the relation between the direction of the charged particle and the emitted Cherenkov photons. The total number of emitted Cherenkov photons is used to reconstruct the momentum of each particle, which is known to have good correlation with the neutrino momentum. The emission of Cherenkov photons starts from the interaction point. Therefore, it is possible to reconstruct the vertex by using the timing information. The shapes of the Cherenkov images are different for different kinds of the particles. For example, electrons and gammas, which generate electromagnetic showers, create rather diffuse Cherenkov images. By using these differences in the images, we can identify the types of particles. Therefore, we need to record both timing and charge from each PMT. For that purpose, we have developed a special electronics module, called ATM, to record this information without deadtime. In Super-Kamiokande, we have been using the same 20 inch PMT, high voltage power supply system for the PMTs, and readout electronics. Therefore, the characteristics of this equipment is well understood.

This detector generates the trigger by itself, using the number of hit PMTs within a 200 ns window, and then records the event. However, there is no earth shield for the cosmic-ray muons. Therefore, it is necessary to supply a global gate signal to avoid recording such unnecessary events. For that purpose, we prepared a global gate signal, called the spill gate, which is provided by the accelerator and whose width is adjusted based on the width of a spill. A difference from the Super-Kamiokande detector is that we also record the numbers of hit PMTs with FADC modules. This information is useful for counting the number of interactions in an event or a spill. The average number of visible interactions in a spill has been estimated, and was observed to be about 0.2. Thus about 10% of the spills have more than one interaction. Therefore, we set the threshold at 1000 photoelectrons (p.e.) to count the number of peaks in the FADC. This threshold corresponds to about 100 MeV electron equivalent energy. There are also events caused by the decay electrons from cosmic-ray muons, which stop in the detector. Some of these decay electron events, whose parent muons came into the detector just before the spill gate, cannot be eliminated only by the information from the ATM modules. Therefore, we need to use the data from the FADC to reject these events.

We apply the following criteria to select the neutrino-induced events for the estimation of the absolute neutrino flux:

a) there was no detector activity in the 1.2 μsec preceding the beam spill,

b) only one peak was recorded in the FADC,

c) the reconstructed vertex must be in the fiducial volume.

We define a cylindrical fiducial volume along the beam direction whose radius is 2 m and whose length is 4 m. Criterion a) removes events which were caused by electrons from the decay of cosmic-ray muons. Criterion b) removes events with more than one interaction. In criterion c), we defined a rather small fiducial volume in order to remove the cosmic-ray muons and to reduce the systematic errors coming from the vertex resolution. The reconstructed vertex distributions just before criterion c) was applied are shown in Fig. 14 and agree with the Monte Carlo.

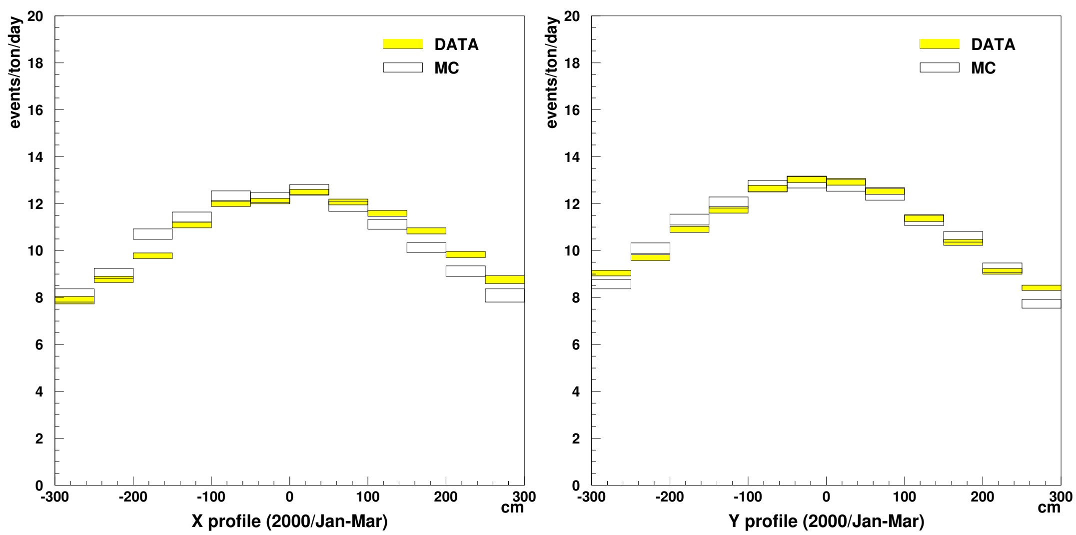

(A) (B)

Fig. 14. (A) Horizontal and (B) vertical vertex distributions of neutrino interactions in the 1 kt water Cherenkov detector. The open boxes show the data and the shaded boxes show the Monte Carlo. The vertical size of each box corresponds to the statistical error.

Fig. 15 shows the the stability of the event rate and it is very stable as expected. In June '99, the configuration of the target and horns was different, as described above, and in November '99, the detector configuration was slightly different from the other periods. Therefore, the event rate is slightly lower during these periods.

By applying all the neutrino event selection cuts to the generated Monte Carlo events, detection efficiencies were estimated to be 86% for the charged current interactions and 33% for the neutral current interactions. Combining all the interactions, the estimated detection efficiency of the 1 kt detector is 71%.

4.4 Expected number of events at Super-Kamiokande

In order to obtain the expected number of events at Super-Kamiokande, we use the following method. First, we use the Monte Carlo simulation to obtain the neutrino spectrum. The energy spectrum of this Monte Carlo has been guaranteed by the results

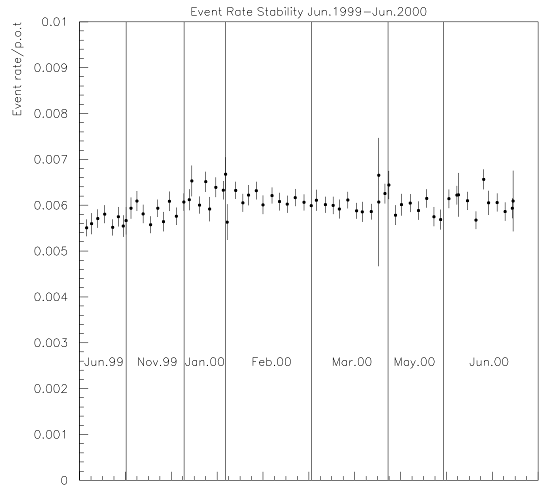

Fig. 15. Time dependence of the neutrino event rate observed at the 1 kt water Cherenkov detector. Each point represents an average of 5 days. The error bars show the statistical errors.

from the pion monitor measurement shown in Fig. 6. For the absolute normalization, we use the number of events observed in the front neutrino detectors. We have generated Monte Carlo events, passed them through the event selections, and obtained the absolute normalization factors of our neutrino fluxes by comparing the observed numbers of events from the front neutrino detectors. Then, we can calculate the expected number of events at Super-Kamiokande. The actual formula to obtain the expected number of events without oscillation is as follows:

$$N_{SK}(\text{expected}) \;=\; N_{FD} \times \frac{\eta_{SK}}{\eta_{FD}} \times \frac{M_{SK}}{M_{FD}} \times \frac{POT_{SK}}{POT_{FD}}, \tag{3}$$

$$\eta \;\equiv\; \int (\phi \times \sigma \times \epsilon)\, dE_{\nu}, \tag{4}$$

where N_{FD} is the observed number of neutrino events at the front detector, η_{SK}/η_{FD} is the Far-to-Near event ratio, $M_{SK}(M_{FD})$ is the fiducial mass of Super-Kamiokande (front) detector, and $POT_{SK}(POT_{FD})$ is the number of protons on target used for the analysis of Super-Kamiokande (front) detector, ϕ is the neutrino flux at each detector, σ is the neutrino cross-section, ϵ is the detection efficiency and E_{ν} is the energy of neutrino, respectively. The expected number of events at Super-Kamiokande, estimated by using the results from the 1 kt detector, is $40.3\,^{+4.7}_{-4.6}$. The major sources of systematic error come from the vertex resolution and the treatment of multiple interactions in a spill. These errors will be reduced soon by refining the vertex fitter and treating the

	1kt water Cherenkov	Muon range detector	Scintillating fiber tracker
Fiducial mass (tons)	50 (H_2O)	312 (Fe)	5.9 (H_2O+Al)
Detection Efficiency	0.71	0.33	0.24
Number of observed ν events	63508	223419	2953
Expected number of events at Super-Kamiokande	$40.3^{+4.7}_{-4.6}$	$41.4^{+6.2}_{-6.4}$	$40.0^{+5.2}_{-5.5}$

Table 1. Summary of expected number of events at Super-Kamiokande

events with multiple interactions more precisely. The systematic error coming from the extrapolation of the neutrino flux from the near measurement to Super-Kamiokande is estimated to be 7%. This error comes from the uncertainty in the measurement of the pion monitor and the Monte Carlo uncertainty for low energy neutrinos. The systematic error from the measurements at Super-Kamiokande is estimated to be 2%, which comes mainly from the uncertainty of the vertex fitting and the fiducial volume cut. The expected numbers of events obtained from the other two near detectors are also summarized in Table 1. All the numbers are consistent within errors.

4.5 Super-Kamiokande

The Super-Kamiokande detector is the world largest ring imaging water Cherenkov detector. It is located 1000 m (2700 m water equivalent) below the peak of Mt. Ikenoyama in the Mozumi zinc mine near Kamioka, Japan. Fifty kilotons of ultra pure water are held within a stainless steel tank of height 41.4 m and diameter 39.3 m. The tank is optically separated into two regions, the inner and anti-detectors, by a PMT support structure covered with a white reflector sheet (Tyvek), and a black sheet. The inner detector has a height of 36.2 m and a diameter of 33.8 m. The anti-detector completely surrounds the inner detector and is used to identify incoming and outgoing particles. On the wall of the inner detector, there are 11,146 50 cm inward-facing PMTs, which cover 40% of the surface. The anti-detector is lined with 1,885 20 cm PMTs equipped with 60×60 cm wavelength-shifter plates to increase the collection efficiency for Cherenkov photons.

In order to select the events at Super-Kamiokande which were generated by the neutrinos from KEK, we use the timing information provided by the GPS system.[17] At the KEK site, we record the absolute timing information of each spill (T(KEK)).

Also we record the timing information for all the events in Super-Kamiokande (T(SK)). Then, we calculate the time differences between the beam spill timing and the trigger timing of the events in Super-Kamiokande. If the neutrino-induced events have a timing difference which is consistent with the time of flight from KEK to Super-Kamiokande (T(TOF)), those events are defined to be events generated by the neutrinos from KEK. The two GPS systems, one placed in KEK and the other located at the Kamiokande site, have been checked with an atomic clock, and the absolute timing difference of these two clocks is obtained to be less than $\pm 100\,\mathrm{ns}$. Therefore, we can set a very narrow timing window. Basically there are no background events to search for the neutrino interactions in Super-Kamiokande, and thus we don't have to worry about the background other than atmospheric neutrino events. In Super-Kamiokande, about 10 atmospheric neutrino events are detected every day. On the other hand, the protons are extracted about 40,000 times per day and we open only 1.4 μs as spill gate for each spill. From there numbers we can easily estimate the probability to misidentify an atmospheric neutrino event as a neutrino beam event, and the probability is less than 1×10^{-5}. Therefore, we can safely assume that the events within the gate are generated by the neutrinos from KEK.

The actual criteria to select the neutrino events at Super-Kamiokande are defined as follows:

a) the timing of the event is consistent with the beam,

-0.1 $\leq$ ΔT ($\equiv$ T(SK)-T(KEK)-T(TOF)) $\leq$ 1.3 μs,

b) there should be no events within 30 μs before the event,

c) the number of photoelectrons in a 300 ns window must be greater than 200,

d) the maximum charge of a PMT in the event must be smaller than 200 p.e.,

e) the number of hit PMTs of the largest cluster in the outer detector should be less than 10,

f) the reconstructed vertex must be in the fiducial volume.

Criterion a) is used to select events which could be generated by the neutrino from KEK. Criterion b) is used to remove events generated by decay-electron s from incoming cosmic-ray muons. Criterion c) is used to remove low energy events. Criterion d) is used to eliminate events in which a particle escaped from the inner detector. Criterion e) is used to reject entering cosmic-ray muons. We have generated Monte Carlo events to estimate the detection efficiencies. The detection efficiencies for charged and neutral current interactions are estimated to be 93% and 42%, respectively, and the overall detection efficiency is estimated to be 79%. Figure 16 shows the distributions of ΔT.

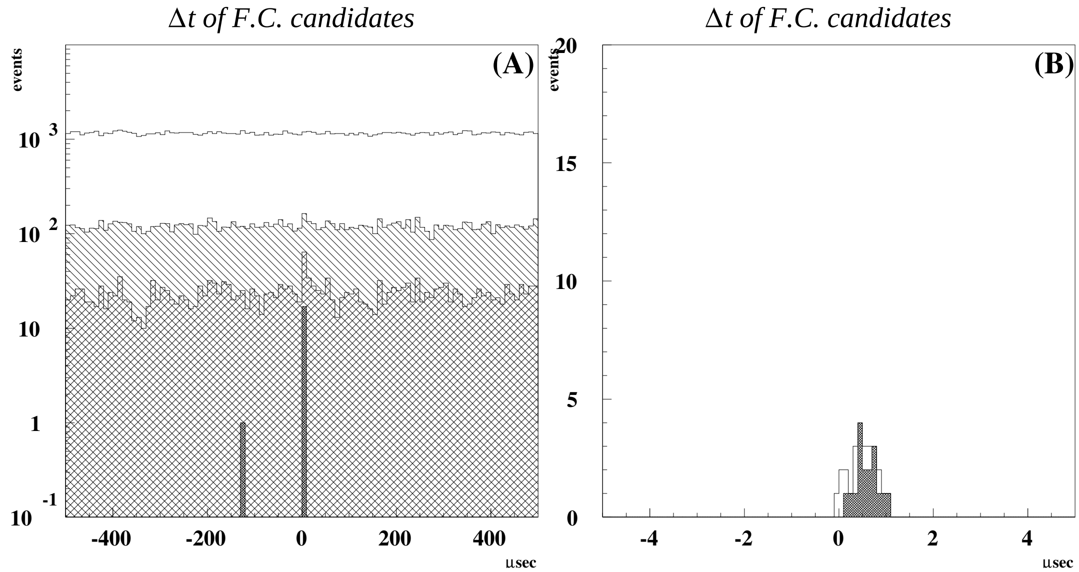

Fig. 16. ΔT ($\equiv T(SK) - T(KEK) - TOF$) distributions. (A) ΔT distributions for $\pm\,500\,\mu$s window. The clear histogram shows the events after the decay-electron cut (criterion b). The hatched histogram shows the events after the HE trigger cut. The shaded histogram shows the events after imposing criterion d. The filled histogram shows the events after the fully-contained cut (criterion e) and the fiducial volume cut. (B) ΔT distributions for $\pm\,5\,\mu$s window. The clear histogram shows all the fully contained events. The filled area corresponds to the fully contained events in the fiducial volume.

In figure 16-(A), we used a rather loose timing cut instead of criterion a). After applying the fiducial volume cuts, there is a clear peak observed around 0 to 1 μs as shown in Figure 16-(B).

There are 27 events observed after applying the 22.5 kt fiducial volume cut, which is the same criterion as for the atmospheric neutrino analysis in Super-Kamiokande. The number of background events is estimated to be less than 10^{-3} events. The expected number of events was 40.3 and the deficit from the expected value is at the 2 sigma level. The detailed numbers of events are summarized in Table 2.

Figure 17 shows various distributions of the observed events. The particle direction of 1-ring μ-like events shown in Fig. 17-(B) seems to have a good correlation with the direction of the neutrino from KEK, as expected. However, the statistics are so low that it is impossible to say something conclusive.

# of observed events and expected events			1999/06-2000/06		
			$\Delta m^2 (\times 10^{-3} eV^2)$		
	Obs.	Exp.	3	5	7
FC 22.5kt	27	$40.3\ ^{+4.7}_{-4.6}$	$26.6\ ^{+3.4}_{-3.3}$	$17.8\ ^{+2.3}_{-2.2}$	$14.9\ ^{+1.9}_{-1.9}$
1-ring	15	24.3±3.6	14.4±2.3	9.4±1.5	8.6±1.4
μ-like	14	21.9±3.5	12.4±2.1	7.5±1.3	6.8±1.2
e-like	1	2.4±0.5	2.1±0.4	1.9±0.4	1.8±0.4
multi ring	12	16.0±2.7	12.2±2.1	8.4±1.5	6.3±1.1
out-of-FV	16	17.2	11.2	7.6	6.7

Table 2. Observed and expected number of events.

5 Summary

The K2K experiment, which is the first accelerator-based long baseline neutrino oscillation experiment, was successfully started in March 1999. All the equipment has been aligned to an accuracy of 0.1 mrad, which is sufficient for this experiment. The accumulated number of protons delivered on target is 2.29×10^{19}. The beam has been monitored spill by spill by the muon monitors and is well controlled and the direction of the beam is well centered within 1 mrad for both vertical and horizontal directions throughout the experimental period. The pion monitor also works well and we obtained the distributions of momentum and direction of pions just after the target. The neutrino fluxes at both near and far sites, obtained from the pion monitor, are well reproduced by our Monte Carlo simulation. Also, the neutrino detectors at the near site have been working fine. We have monitored the profile and the direction of the neutrino beam with the muon range detector. The time variation of the spectrum of the neutrino beam has also been monitored and it was found to be stable. The expected number of events at Super-Kamiokande was estimated by using the results from the 1 kt water Cherenkov detector, and it was $40.3^{+4.7}-4.6$. The expected numbers of events at Super-Kamiokande are also calculated based on the results from the other two detectors, the muon range detector and the scintillating fiber tracking detector. As a result, all the numbers are consistent within the errors. We have observed 27 events at Super-Kamiokande, which is 2 sigma off from the expected number of events. It is planned to run for few more years and the total number of protons on target will reach 1.0×10^{20}, which is 5 times larger than the current statistics.

We gratefully acknowledge the cooperation of the Kamioka Mining and Smelting Company. This work has been supported by the Ministry of Education, Science, Sports and Culture, Government of Japan, US Department of Energy and the Korean Ministry of Science.

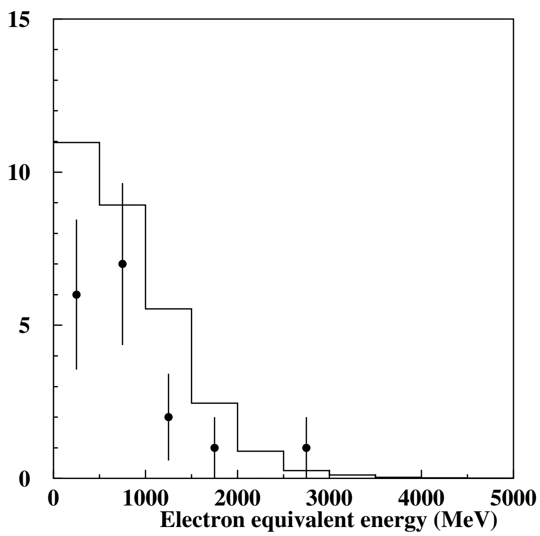

(A)

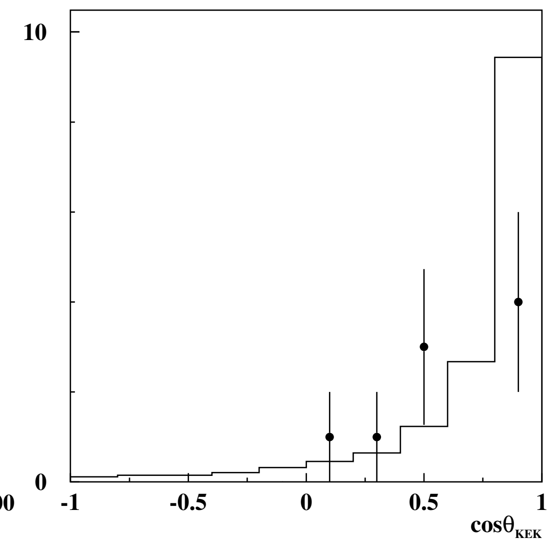

(B)

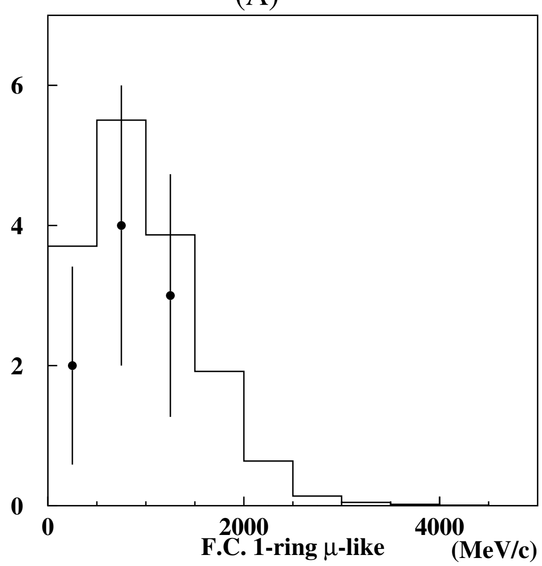

(C)

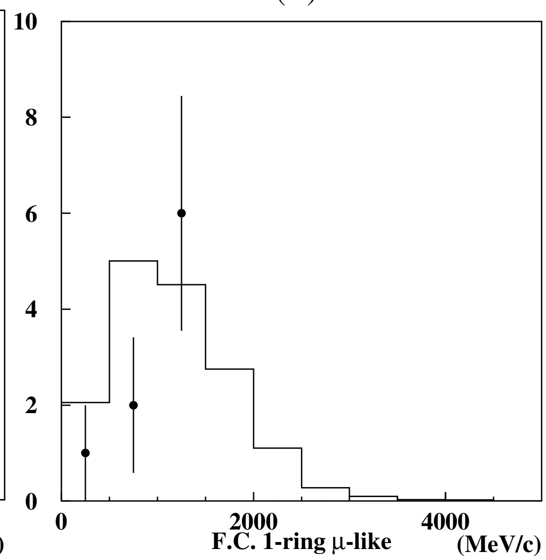

(D)

Fig. 17. Various distributions of K2K neutrino events observed at Super-Kamiokande. (A) Electron equivalent energy of all the fully contained events. (B) Opening angle between the direction of the neutrino and the observed muon. (C) Reconstructed momentum of the muon. (D) Reconstructed energy of ν assuming quasi-elastic scattering. We used the fully contained 1-ring μ-like events for figures (B) to (D). The open circles show the data and each error bar shows the statistical error. The solid histograms show the expectation assuming that there is no oscillation.

References

[1] S. Glashow, Nucl. Phys. **22**, 59 (1961);
S. Weinberg, Phys. Rev. Lett. **19**, 1264 (1967);
A. Salam, Elementary Particle Physics, ed. by N. Svartholm, Stockholm, Almquist and Wiksell (1968).

[2] K.S. Hirata *et al.*, Phys. Lett. **B205**, 416 (1988);
K.S. Hirata *et al.*, Phys.Lett. **B280**, 146 (1992);
Y. Fukuda *et al.*, Phys. Lett. **B335**, 237 (1994).

[3] D. Casper *et al.*, Phys. Rev. Lett. **66**, 2561 (1991);
R. Becker-Szendy *et al.*, Phys. Rev. **D46**, 3720 (1992).

[4] W.W.M. Allison *et al.*, Phys. Lett. **B391**, 491 (1997);
W.W.M. Allison *et al.*, Phys. Lett. **B449**, 137 (1999).

[5] Y. Fukuda *et al.*, Phys. Lett. **B433**, 9 (1998);
Y. Fukuda *et al.*, Phys. Lett. **B436**, 33 (1998);
Y. Fukuda *et al.*, Phys. Rev. Lett. **81**, 1562 (1998).

[6] K. Nishikawa, Nucl. Phys. B. (Proc. Suppl.) **77**, 198 (1999).

[7] M. Ieiri *et al.*, Proc. 1st Asian Pacific Accelerator Conference, 579 (1998).

[8] H. Sato, Proc. Particle Accelerator Conference (1999);
K. Takayama, ICFA Beam Dynamics Newsletter No. 20 (1999).

[9] Y. Yamanoi *et al.*, Proc. 15th International Conference on Magnet Technology (1997);
Y. Yamanoi *et al.*, IEEE Transactions on Applied Superconductivity **10**, 252 (2000);
Y. Suzuki *et al.*, Proc. International Conference on Accelerator and Large Experimental Physics Control Systems (ICALEPCS) (1997);
Y. Suzuki *et al.*, Proc. of ICALEPCS (1999).

[10] H. Noumi *et al.*, NIM **A398**, 399 (1997).

[11] T. Maruyama, Ph.D. Thesis, Tohoku University (2000).

[12] R. Brun *et al.*, CERN DD/EE/84-1 (1987).

[13] J.R. Sanford and C.L. Wang, BNL AGS internal reports No. BNL11299 and No. BNL11479 (1967);

C.L. Wang, Phys. Rev. Lett. **25**, 1068 (1970);
Y. Cho *et al.*, Phys. Rev. **D4**, 1967 (1971);
J.G. Asbury *et al.*, Phys. Rev. **178**, 2086 (1969);
G.J. Marmer *et al.*, Phys. Rev. **179**, 1294 (1969);
G.J. Marmer and D.E. Lundquist, Phys. Rev. **D3**, 1089 (1971);
J.V. Allaby *et al.*, CERN-TH-70-12 (1970).

[14] T.A. Gabriel *et al.*, ORNL/TM-11185;
C. Zeitnitz and T.A. Gabriel, NIM **A349**, 106 (1994).

[15] A. Suzuki *et al.*, NIM **A453**, 165 (2000).

[16] K2K collaboration, to be published.

[17] H.G. Berns and R.J. Wilkes, IEEE NS **47**, 340 (2000).